Vol. 63: 19–30, 2015
doi: 10.3354/cr01284

CLIMATE RESEARCH
Clim Res

Published online March 18

Secular non-linear trends and multi-timescale oscillations of regional surface air temperature in eastern China

Kaijun Wu, Weihong Qian*

Department of Atmospheric and Oceanic Sciences, School of Physics, Peking University, Beijing 100871, PR China

ABSTRACT: Secular trends and multi-timescale oscillations of global and regional surface air temperature (SAT) have been widely investigated in recent decades. In this paper, the method of ensemble empirical mode decomposition (EEMD) is first used to decompose 18 station SAT anomalies in eastern China from 1921 to 2011; 16 stations are then grouped into 4 regions based on the secular non-linear trend and multi-timescale oscillations longer than 10 yr in these SAT anomaly series. The analysis showed that multi-timescale oscillations commonly exist in eastern China, while the 2 largest regional warming trends of 3.3 and 1.21°C per century exist in Northeast China and North China, respectively. Four regional secular non-linear trends and multi-timescale oscillations were explained and used in the extrapolation for the coming 2 decades. Although there is a secular warming trend, the predicted SAT anomaly for Northeast China is expected to continue the recent warming slowdown in this decade and then a new warm flat in the following decade. For other regional SAT anomaly predictions, North China will have a slight warming trend in the coming 2 decades, central China will have a warming process in this decade then a new warm spell in the 2020s, and South China will maintain the current level in this decade then have a quick warming process in the 2020s.

KEY WORDS: Secular trend · Multi-timescale variability · Surface air temperature · Eastern China · Climate prediction

1. INTRODUCTION

The observed warming rate of the surface air temperature (SAT) is non-uniform in multiple spatial patterns and multiple time scales. After a cooling period in the 1960s and 1970s, the global warming has been accelerating (Stocker et al. 2013). Most recent speculations concerned a possible 'hiatus' or 'decade-long stagnation with a flat' of the warming rate of the global-mean SAT (e.g. Kerr 2009, W. H. Qian et al. 2010, Foster & Rahmstorf 2011, Kosaka & Xie 2013). For the basic feature of global-mean SAT, 3 warming rates of 0.44, 0.73, and 1.7°C per century from different durations of 1850–2008, 1911–2008, and 1976–2008 as well as 3 warm spells and 2 cool spells that peaked around the years of 1878, 1911, 1944, 1976, and 1998 were analyzed by separating secular linear trends and inter-decadal variations (W. H. Qian et al. 2010). Similar secular trends were also detected recently by Tung & Zhou (2013) and Zhou & Tung (2013). It was confirmed that climate change includes a secular trend and short-term oscillations (Gao et al. 2006). Climate trends were different in the 2 hemispheres and various continents (Stocker et al. 2013). Even in eastern China, secular trends of SAT are different in southern and northern China (S. W. Wang et al. 2004, Y. G. Wang et al. 2005, Pu et al. 2007).

Multi-timescale variability exists not only in the global-mean SAT but also in the Chinese SAT (W. H.

*Corresponding author: qianwh@pku.edu.cn

Qian et al. 2010, C. Qian et al. 2010, Fu et al. 2011). The global-mean SAT showed that the current hiatus may be part of natural climate variability, tied specifically to a La Niña-like decadal cooling (Kosaka & Xie 2013). In recent years, multi-timescale variability of global and regional SATs were widely studied (e.g. Delworth & Mann 2000, Barlow et al. 2001, Rayner et al. 2003, Li & Bates 2007, Wang et al. 2009, Hoerling et al. 2011, Li et al. 2012). These studies showed that the attribution of multi-timescale climate variability is mainly associated with natural oscillations of sea surface temperature (SST) in 3 basins of the Pacific, Atlantic, and Indian oceans. It was noted that the Atlantic multi-timescale oscillation (AMO) has a period of ~65 yr and amplitude of ~0.4°C (Delworth & Mann 2000, Enfield & Trimble 2001, Sutton & Hodson 2007). The Pacific decadal oscillation (PDO) was observed to have decadal and inter-decadal timescales of around 20 and 50 yr, respectively (Mantua et al. 1997, Barlow et al. 2001). There is also inter-decadal climate change over the Indian Ocean region (Allan et al. 1995, Li et al. 2012). The decadal phase differences of these natural oscillations related to the Northern Hemisphere mean SAT anomalies were also investigated by Li et al. (2013).

Decadal climate prediction has become a new research field (e.g. Meehl et al. 2009, Hurrell et al. 2010, Murphy et al. 2010) and was listed as a key component of the fifth IPCC assessment report (Taylor et al. 2012). Most predictions were made by global climate models (e.g. Smith et al. 2007, Keenlyside et al. 2008, Pohlmann et al. 2009, Mochizuki et al. 2010, Hoerling et al. 2011, Wang et al. 2013). Many models are able to simulate historical secular trends in the last century, but their ability to simulate inter-decadal variability is weak (Fu et al. 2011). The uncertainty of inter-decadal climate prediction is based on the lack of not only observational coverage, imperfect assimilation techniques, and model climatic shifts but also the basic limitations and imperfections of climate models themselves (Stainforth et al. 2007). Using the Statistical Regional Model, Zhu et al. (2013) predicted that the spatial average temperature in the Tibetan Plateau will increase by 0.68 to 0.98°C for the period 2015 to 2050 and described more details of the seasonal variations. Thus, statistical or empirical approaches based on physical understanding may be a valid alternative for decadal climate prediction. A simple empirical approach was applied by Gao et al. (2006) using a secular linear trend of the global-mean SAT from 1860 to 2000 overlapping with an inter-decadal oscillation. The decadal prediction using this linear trend and oscillation showed that a cooling trend was expected from 1998 to 2030, i.e. the current warm flat was successfully predicted. Following this empirical approach, W. H. Qian et al. (2010) took a secular linear trend of the global-mean SAT from 1850 to 2008 and 2 cosine functions with 2 quasi-periods of 21.2 and 64.1 yr to predict that a cool spell with a following warm spell is expected in the early 2030s and the late 2050s, respectively. The effectiveness of this empirical approach relied on how well a secular trend could be established and how many quasi-periodic oscillations could be extracted and applied. Recently, Fu et al. (2011) adapted a method of ensemble empirical mode decomposition (EEMD) to decompose the global-mean SAT into multi-timescale components and a secular non-linear trend. It is understood in these studies that the natural oscillations and anthropogenic warming are commonly considered to compose the observed climate change.

An accurate prediction of future SAT change requires reliable historical records from which substantial variations of SAT could be identified and the underlying causes of the changes could be accurately understood. In this paper, we mainly focus on the identification of some quasi-periodic oscillations by decomposing a set of reliable observational records into several components through the EEMD method and then extrapolating future SAT-anomaly tendencies in eastern China. The dataset and the method of extracting the multi-timescale variability from the SAT anomaly in eastern China are introduced in Sections 2 and 3, respectively. Historical decompositions and future extrapolations of 4 regional SAT-anomaly time series in eastern China are conducted in Section 4. Finally, conclusions and discussion are given in Section 5.

2. DATA AND METHODOLOGY

2.1. Temperature data

Long-term instrumental SAT data in China have been collected, compiled, and constructed over decades. Collections of the early observational temperature in China were made mostly in the 1990s (e.g. Wang 1990, Tao et al. 1991, R. S. Wang et al. 1991, Tang & Lin 1992, Lin et al. 1995, S. W. Wang et al. 1998). These studies addressed the early sparse instrumental observations in China before 1950, including a number of missing records. One important fact noticed in these reports was that some stations did not follow a consistent observational schedule. Although a national surface meteorological observa-

tion network with >2000 stations had been established in China from 1950, ~80% of these stations have been relocated at least once. One of the reasons for relocations is the growth and expansion of cities, particularly for those stations across eastern China over the past 3 decades. These changes in station positions and types of thermometers will probably cause significant inhomogeneities in the secular SAT series and potentially add uncertainty to the estimation of SAT trends in China (Yan et al. 2001). Both the missing records and the inhomogeneous data may hinder the construction of homogeneous SAT time series in China. Cao et al. (2013) used only 18 stations in eastern China to obtain a complete set of useful observational surface series. In that work, some missing and inhomogeneous records were interpolated and replaced using 3 methods: an integrated method, gradient plus inverse distance square, and relaxed integrated method. The error estimation of a cross validation of the interpolation methods at 18 stations was reported in detail by Cao et al. (2013) in their Table 2. Only 5 stations have entire monthly-mean temperature series among the 18 stations, while the other 13 stations have missing records of 32 to 134 months. Now, this dataset of the monthly-mean instrumental SAT anomaly at 18 stations across eastern China (Fig. 1) since the late 19th century or early 20th century has been updated using these methods and can be downloaded from the National Meteorological Information Center (NMIC) of the China Meteorological Administration (http://cdc.cma.gov.cn). In Fig. 1, the longest monthly-mean SAT series is at the Shanghai (East China) station starting from January 1873, while the shortest monthly-mean SAT series is at the Kunming (Southwest China) station starting from January 1921. In 1921, there were 18 stations in total located in eastern China, with 4 stations in South China, 6 stations along the Yangtze River, 5 stations in North China, and 3 stations in Northeast China, which are mostly located in rapidly developing or large cities. In the present study, the updated annual-mean SAT series by Cao et al. (2013) at the 18 stations from 1921 to 2011 are used to analyze their secular trend and multi-timescale variability.

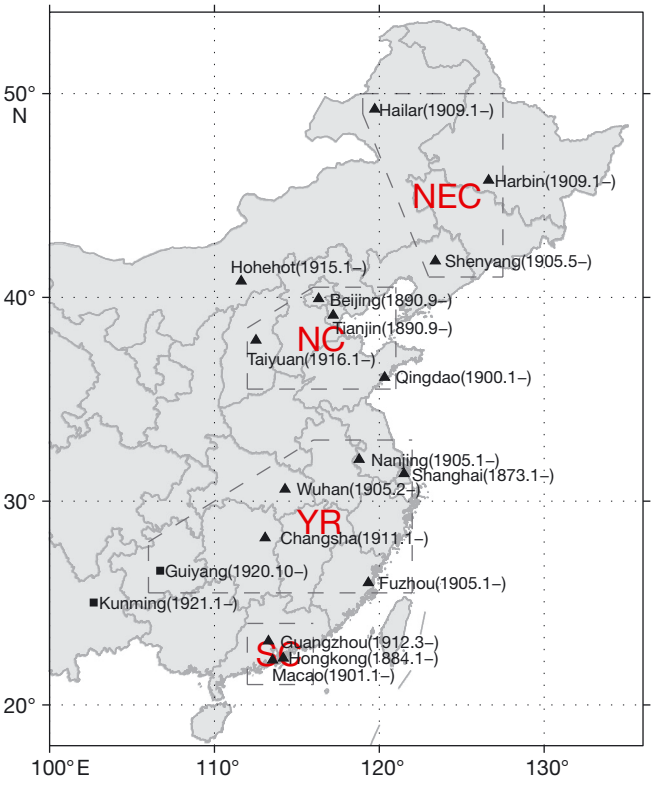

Fig. 1. Locations of 18 stations in China: 16 stations are separated into 4 basin groups: Northeast China (NEC) with stations of Hailar, Harbin, and Shenyang; North China (NC) with stations of Beijing, Tianjing, Taiyuan, and Qingdao; central China and the valley of the Yangtze River (YR) with stations of Shanghai, Nanjing, Wuhan, Changsha, Fuzhou, and Guiyang; and South China (SC) with stations of Guangzhou, Hong Kong, and Macao. Two stations of Hohehot and Kunming are respectively located over the Inner Mongolian Plateau and the Yunnan-Guizhou Plateau

2.2. Methodology

Two methods are applied in this study. The basic method is the EEMD developed by Wu & Huang (2009) from the original empirical mode decomposition (EMD) proposed by Huang et al. (1998). The EMD provided an adaptive time-frequency data analysis method. The generic principle of EMD is to decompose any time series into a set of intrinsic mode function (IMF) components of the data itself, based on scale separation. The EEMD was developed to add white noise, thus eliminating mode mixing. The time-varying trend in global-mean SAT series was detected by Wu et al. (2011) using the EEMD method. The EEMD is also used in this study to decompose an observational SAT anomaly series into a set of secular non-linear trend and multi-timescale oscillations. An empirical approach applied by Bordi et al. (2004), Gao et al. (2006), W. H. Qian et al. (2010), and Fu et al. (2011) is also used to empirically simulate the past temperature evolutions and extrapolate their future tendencies regarding SAT anomalies in eastern China. By the empirical approach, a set of sine functions and polynomial functions is chosen to simulate and extrapolate decadal and

inter-decadal IMF components as well as the secular non-linear IMF component separated from SAT anomaly time series. To avoid the boundary effect of EEMD, the first and last 3 values of each component are removed from all analyses, including the simulations and predictions after decomposition. During every process of EEMD in the study, the ratio of the standard deviation of the added noise to that of targeted time series is 1, and the ensemble size is 10 000 members.

3. DECOMPOSING SERIES

3.1. Hailar series

To identify the secular non-linear trend and multi-timescale variability, the temperature anomaly series during 1921–2011 at Hailar, the northernmost station of the 18 stations considered in eastern China, is first to be decomposed by the EEMD method as an example (Fig. 2a). The SAT anomaly series is decomposed into 6 IMF components. Each component except for the IMF_6 is characterized as neither a regular oscillation nor irregular oscillation, so we refer to it as quasi-periodic oscillation. Thus, 5 quasi-periodic oscillations including 2 inter-annual oscillations (Fig. 2c,d), 1 decadal oscillation (Fig. 2e), 2 oscillations with their timescales longer than 10 yr (Fig. 2f,g), and a secular non-linear trend (Fig. 2h) from 1924 to 2008 can be identified. The secular non-linear trend indicates that the SAT anomaly at the Hailar station for the past 91 yr (1921–2011) has increased by 2.88°C with an approximately linear trend of 3.16°C per century. This trend is larger than the average trend (1.52°C per century) of the 16 stations in eastern China (Zhao et al. 2014). The centennial-scale trend is usually considered as an influence of human activities on climate change (Salinger 2005, Fu et al. 2011).

With the 34.9% ratio of the standard deviation (SD) of IMF_6 to the sum of SDs of all the components, the secular non-linear trend (IMF_6 in Fig. 2h) can be simulated by a polynomial function and extrapolated for its future 2-decadal tendency. The component of IMF_5 may be a part of an inter-decadal oscillation (Fig. 2g) with a 8.4% ratio, but its time-scale cannot be predetermined due to the limitation of the series length (85 yr). For this situation, it is also treated as a secular non-linear trend simulated by a polynomial function and extrapolated for its future 2-decadal tendency. A long inter-decadal quasi-periodic oscillation (IMF_4 in Fig. 2f) shows 3 entire warm spells that peaked in the early 1930s, near 1960, and the 1990s with a 10.9% ratio. This quasi-periodic oscillation similar to the PDO timescale is also expected to continue in the coming decades, so we use a sine function to simulate this component series and extrapolate its future 2-decadal tendency. The decadal oscillation in IMF_3 (Fig. 2e) shows 7 peaks of variation with a 10.2% ratio of its standard deviation to the sum of the SDs of all the components from 1924 to 2008. This quasi-periodic oscillation, which may correspond to the 11 yr timescale of solar activities (Scafetta & West 2008, Qian & Lu 2010), can be expected to appear in the coming decades, so we use a sine function to simulate this component series and extrapolate its future 2-decadal tendency. Fig. 2c,d illustrate 2 inter-annual oscillations with ratios of

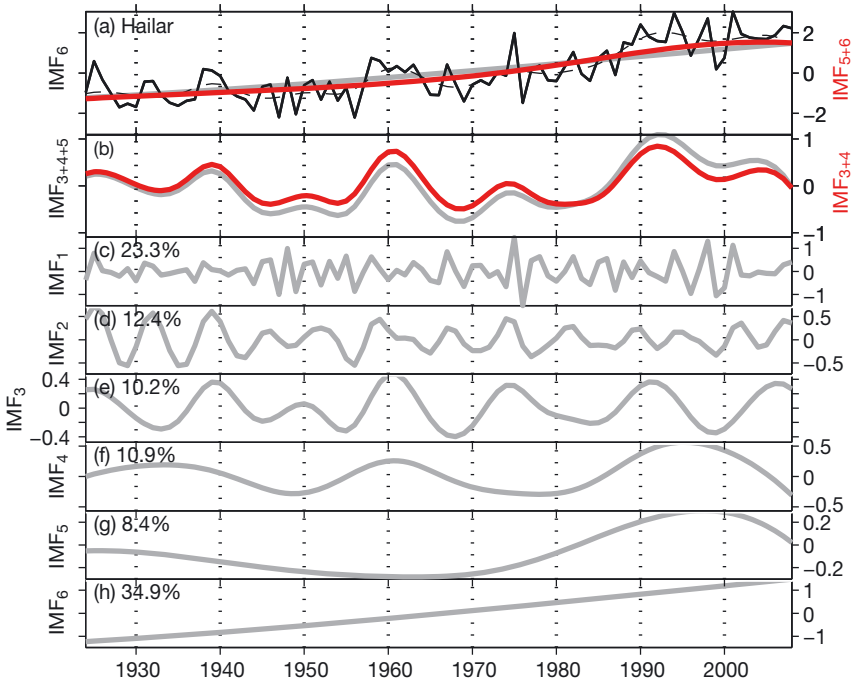

Fig. 2. The original annual-mean SAT anomaly series (°C) at the Hailar station and 6 IMF components of the ensemble empirical mode decomposition (EEMD) from 1924 to 2008. In (a): the black line is the original SAT anomaly series, the thin dashed line is the sum of the IMF_3, IMF_4, IMF_5, and IMF_6 components, and the thick grey and red lines are the IMF_6 component and the sum of IMF_5 and IMF_6 components, respectively. In (b): the thick grey line is the sum of IMF_3, IMF_4, and IMF_5 components, while the thick red line is the sum of the IMF_3 and IMF_4 components. (c–g) Six single components from IMF_1 to IMF_6, respectively. The percentages are the ratio of standard deviation of every component to the sum of all SDs

23.3% and 12.4%. These 2 oscillations may be caused by regional influences. We are here mainly concerned with timescales longer than a decade, so these 2 components are not considered in the following analysis.

Two quasi-periodic oscillations for the SAT series in Hailar are concentrated in 2 components of IMF_3 to IMF_4. The sum of IMF_3 and IMF_4 components is plotted by the red line in Fig. 2b, in which the quasi-periodic oscillation is not as clear as that in each individual component series. In an individual decade, the warm flat becomes very large when the 2 peaks of oscillation overlap, such as near the year 1960 and in the 1990s. Although the ratio of IMF_5 is the smallest among the 6 components, it can modify the amplitude of 2 inter-decadal SAT components, as shown by the thick grey line in Fig. 2b.

The secular non-linear trend of IMF_6 and the sum of 2 secular non-linear trends of IMF_5 and IMF_6 are respectively shown by the thick grey line and the thick red line in Fig. 2a. These two lines have a similar trend fit with the instrumental series. Combining the 2 secular non-linear trends (IMF_5 and IMF_6) and the 2 multi-timescale components (IMF_3 and IMF_4) could account for 64% of the total standard deviations. Similar decompositions and analyses are also processed for other 17 stations with SAT anomaly series in eastern China.

3.2. Grouping series

In a similar way as described for Fig. 2, the other 17 station series are individually analyzed by the EEMD approach. We are only concerned with their secular non-linear trends (IMF_6) and 3 other components (IMF_3, IMF_4, and IMF_5). Fig. 3 illustrates the results. In Fig. 3a, 3 consistent secular non-linear trends are found from the 3 stations of Shenyang, Harbin, and Hailar in Northeast China. Their average warming linear trends in Northeast China are ~3.3°C per century. The other 4 curves of secular non-linear trend belong to the stations of Qingdao, Taiyuan, Tianjin, and Beijing in North China. Before the 1950s, these stations experienced a slight cooling trend and then a warming

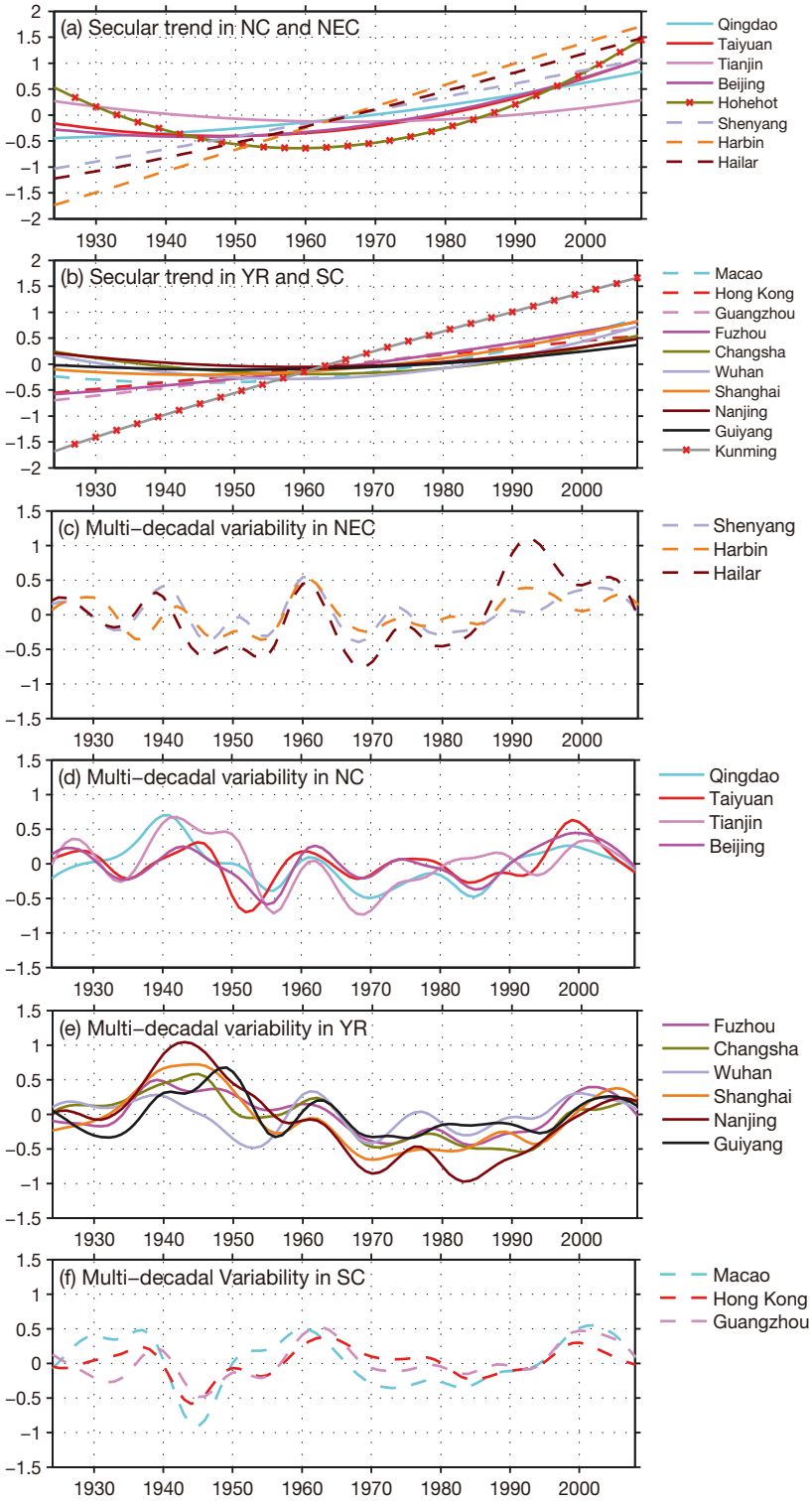

Fig. 3. Secular non-linear trend components of decomposed SAT anomaly (°C) at (a) 8 stations and (b) 10 stations from 1924 to 2008. Combined 3 component series (IMF_3 + IMF_4 + IMF_5) of decomposed SAT anomaly (°C) at (c) 3 stations in Northeast China (NEC; the valley of Songhua River), (d) 4 stations in North China (NC; the valley of lower Yellow River), (e) 6 stations in central China (YR; the valley of Yangtze River), and (f) 3 stations in South China (SC; the valley of Pearl River)

trend since the 1960s. The warming trends at Beijing and Taiyuan are larger than that at Tianjin because the Tianjin station is near the Bohai Sea. The influence of urbanization on the warming trend is larger at the Beijing urban station than at the Beijing rural and mountain stations (Qian & Li 2012). In the present study, the long-term SAT anomaly series of Beijing belongs to one of the urban stations. In contrast, the SAT anomaly of Hohehot station, which is located over the Inner Mongolian Plateau at 1063 m above sea level, shows a strong cooling trend before the 1950s and the strongest warming trend since the 1970s. Fig. 3b gives 9 consistent secular non-linear trends except for only 1 station of Kunming, which shows a significant warming linear trend with the value of 3.97°C per century. The warming trend of Kunming station is similar to that of Harbin, but these stations are respectively located in Southwest China and Northeast China. Among the 18 stations, 6 stations showed weak warming linear trends with values of 0.013°C per century in Tianjin, 0.32°C per century in Nanjing, 0.34°C per century in Changsha, 0.45°C per century in Guiyang, 0.66°C per century in Wuhan, and 1.1°C per century in Shanghai. The stations of Nanjing, Changsha, Guiyang, Wuhan, and Shanghai are located along the Yangtze River, in contrast to the Tianjin station.

The multi-timescale variability of annual-mean SAT anomalies with timescales longer than 10 yr at the 18 stations are given in Fig. 3c–f. The sum series from the 3 components (IMF_3, IMF_4, and IMF_5) at each of the stations of Shenyang, Harbin, and Hailar are pictured in Fig. 3c. There are ~7 peaks in each of the sum series from 1924 to 2008. The largest warm peak of about +1.1°C is noted in the 1990s at the station of Hailar. The amplitude of multi-timescale variability is ~0.5°C in Northeast China. Fig. 3d shows 4 series of summing the 3 inter-decadal components respectively at the stations of Qingdao, Taiyuan, Tianjin, and Beijing in North China. There are ~5 warm peaks with amplitudes of ~0.5°C in Fig. 3d. The 6 stations of Fuzhou, Changsha, Wuhan, Shanghai, Nanjing, and Guiyang are located near the Yangtze River in central China, with their multi-timescale components illustrated in Fig. 3e. The first large warm peak commonly occurred in the 1940s, and the second warm peak was in the last decade. Finally, the 3 stations of Macao, Hong Kong, and Guangzhou are located in South China. Their multi-timescale components are given in Fig. 3f, with 2 warm peaks of about +0.5°C around 1962 and 2002 and a cool peak of about −0.5°C around 1944.

From the analysis of secular non-linear trends and multi-timescale variability at the 18 stations, we found that the former has a maximum rate of ~0.4°C per decade (Fig. 3a), and the latter has a maximum rate of ~1.5°C per decade (Fig. 3c). This implies that for the centennial-scale prediction, the former should have a larger contribution to the future climate change, while for the coming 2 decades, both of them but particularly the latter need to be fully considered. These stations are scattered in the 4 basins: the Songhua River in Northeast China, the lower Yellow River in North China, the Yangtze River in central China, and the Pearl River in South China. We cannot obtain their accurate temporal-spatial principle components based on this north–south oriented distribution of the stations. However, these stations can be divided into 4 groups based on their geographical locations (the 4 basins) and their internal structures of SAT anomaly variability. Among them, 2 stations—Hohehot located over the Inner Mongolian Plateau and Kunming over the Yunnan-Guizhou Plateau—are removed from the 4 groups because their secular trends are different from their adjacent stations, as described in Fig. 3a,b.

4. EXTRAPOLATING PREDICTION

4.1. Test

Before simulating and predicting each group's SAT anomaly, we first check this approach's validity using the combined-mean SAT anomaly series of 3 stations in the Northeast China group (Fig. 4a) by using the series of 1921 to 1990 to predict the future series in the recent 2 decades. The simulation and prediction of the IMF_3 component is shown in Fig. 4c. The grey line is the IMF_3 component from 1924 to 1987, while the dashed line is the fitting curve with 1 sine function for decadal (or inter-decadal) simulation.

$$\mathrm{IMF}_D = A + B \times \sin\left(\frac{2\pi}{T}t\right) \quad (1)$$

Here, the subscript D denotes a decadal (or inter-decadal) IMF component. The fitting function and the IMF_3 component show a correlation 0.67 during 1924 to 1987 when $A = -0.0168$, $B = 0.2653$, and $T = 16.02$. Similarly, the simulation and prediction of IMF_4 is shown in Fig. 4d with a correlation 0.92 during 1924 to 1987 when $A = -0.0078$, $B = 0.191$, and $T = 30.06$. Adding 2 IMF components ($IMF_3 + IMF_4$) together (Fig. 4b), the correlation between 2 curves is 0.82. Three peaks of multi-timescale variation near the years 1927, 1960, and 1974 are well simulated.

As treated for the IMF_5 component in Fig. 2g, the fitting period of IMF_5 is also longer than the series

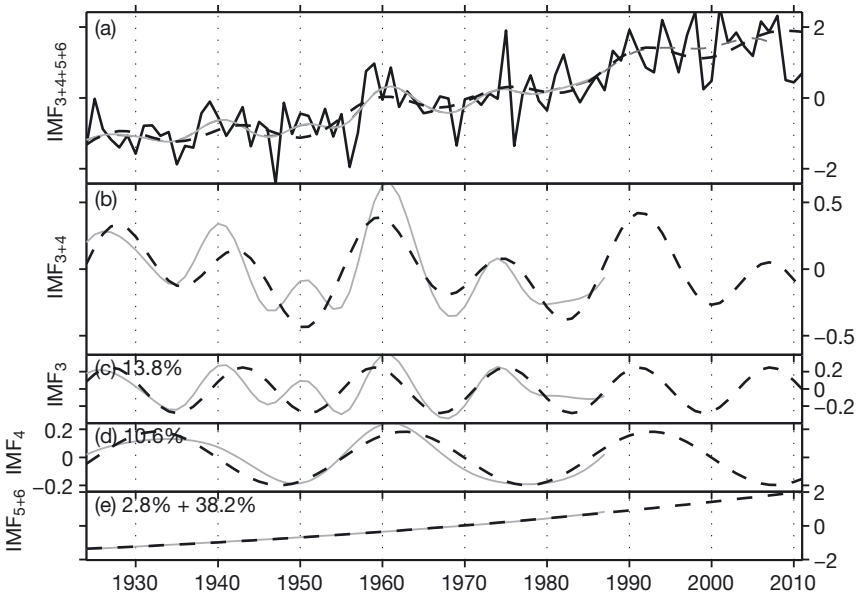

Fig. 4. (a) The original annual-mean SAT anomaly series (black solid line) averaged using 3 station series of Hailar, Harbin, and Shenyang from 1924 to 2011, a combined series of IMF_3, IMF_4, IMF_5, and IMF_6 components from 1924 to 1987 (grey solid line), a prediction following a simulation used 2 sine functions and a 2nd-order polynomial function (black dashed line) from 1924 to 2011, and a combination of IMF_3, IMF_4, IMF_5, and IMF_6 components from 1924 to 2008 (grey dashed line); (b) a combined series of IMF_3 and IMF_4 components from 1924 to 1987 (grey line) and a prediction (1988–2011) following a simulation (1924–1987) using 2 sine functions (dashed line); (c) the IMF_3 component (grey line) and a prediction (1988–2011) following a simulation (1924–1987) using a sine function (dashed line); (d) same as (c) but for the IMF_4 component; (e) a combined series of IMF_5 and IMF_6 components from 1924 to 1987 (grey line) and a prediction (1988–2011) following a simulation (1924–1987) using a 2nd-order polynomial function (dashed line). The percentages are the ratio of standard deviation of every component to the total SDs from 1924 to 1987

length (65 yr) so it is improper to simulate this series using a sine function. Thus, the sum of IMF_5 and IMF_6 as the secular non-linear trend from 1924 to 1987 is simulated by the following 2nd-order polynomial function as plotted in Fig. 4e:

$$\text{Trend} = C_1 + C_2 t + C_3 t^2 \quad (2)$$

The secular non-linear trend is simulated when $C_1 = 763.6980$, $C_2 = -0.8153$, and $C_3 = 0.00021707$.

The final test result, which accounts for 65.4% of the total SDs, is shown in Fig. 4a after summing the multi-timescales components (Fig. 4b) and the secular non-linear trend series (Fig. 4e). The correlation coefficient between the total fitting curve (black dashed line) and combination of 4 components (grey solid line) is 0.96. Although the degree of freedom of the 4 components used reduces after removing 2 inter-annual components (IMF_1 and IMF_2), there are still 6 degrees of freedom calculated by the function of Vondark low-pass filtering or 12 degrees of freedom by that of FFT low-pass filtering while the total sample size is 65 and the cutoff frequency is 1/10 yr. In the former condition, the least correlation coefficient reaching the 99% confidence level is 0.83, while in the latter condition, the least correlation coefficient reaching the 99% confidence level is 0.66. In Fig. 4a, the correlation coefficient of 0.96 between the total fitting curve (black dashed line) and combination of 4 components (grey solid line) reaches the 99% confidence level on both of 2 conditions. A prediction of SAT anomaly depicted by the dashed line in Northeast China is well matched to the combination indicated by the grey dashed line for the period 1987 to 2008 in Fig. 4a.

4.2. Prediction

Using the same procedures as in the above test, a prediction (for 2009 to 2030) following a simulation (1924 to 2008) is made in the group of stations in Northeast China for the next 2 decades. Fig. 5 shows the detailed result. The fitting curve and IMF_3 component show a correlation of 0.73 during 1924 to 2008 when a sine function (Eq. 1) is performed with coefficients of $A = 0.0052$, $B = 0.2354$, and $T = 16.02$ (Fig. 5c). The prediction is made for the following 2 decades (2009 to 2030). Similarly, the simulation and prediction of IMF_4 component are shown in Fig. 5d with their coefficients listed in Table 1. The simulations and predictions of IMF_3 and IMF_4 components are combined in Fig. 5b.

The secular non-linear trend (sum of IMF_5 and IMF_6) from 1924 to 2008 is simulated by a 2nd-order polynomial function (Eq. 2) with $C_1 = 421.2565$, $C_2 = -0.4643$, and $C_3 = 0.00012713$ (Fig. 5e). A prediction of SAT anomaly in Northeast China from 2009 to 2030 is shown in Fig. 5a. Although there is a secular warming trend, the SAT anomaly is predicted to continue the recent warming slowdown in this decade and then exhibit a new warm flat in the next decade. This is because a cool spell following a warm spell is predicted by the multi-timescale variability (dashed line in Fig. 5b). For this group, all coefficients used in the 2 sine functions and the 2nd-order polynomial function as well as the correlations between the sim-

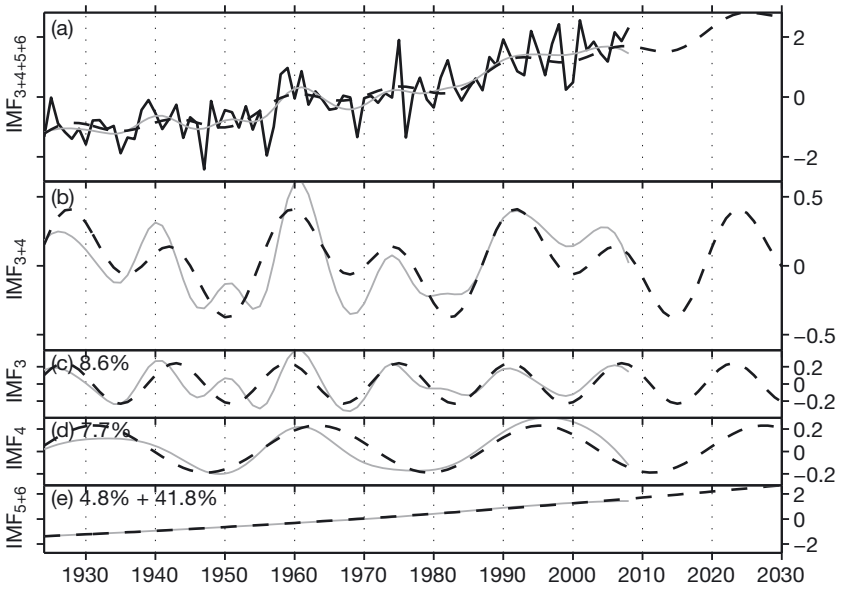

Fig. 5. Same as in Fig. 4 except of the original annual-mean SAT anomaly series averaged from 1924 to 2008 and a prediction from 2009 to 2030 (dashed line)

ulated and original series are listed in Table 1. While the total sample size is 85 and the cutoff frequency is 1/10 yr, the 4 components still have 8 degrees of freedom calculated by the function of Vondark low-pass filtering or 16 degrees of freedom by that of FFT low-pass filtering. In the former condition, the least correlation coefficient reaching the 99% confidence level is 0.77, while in the latter condition, the least correlation coefficient reaching the 99% confidence level is 0.59. The correlation coefficient between the total fitting curve and the sum or combination of 4 components is 0.99 reaching the 99% confidence level on both of 2 conditions.

Similar simulations and predictions for the other 3 groups of SAT anomaly series in North China, central China, and South China are shown in Figs. 6–8, respectively. In their EEMD decomposition, the IMF_5 component clearly shows a sine oscillation in these 3 groups of SAT anomaly series. Thus, 3 sine functions and a 2nd-order polynomial function are used to simulate their combinations (Table 1). In the group of North China, the prediction based on a combinination of the 3 sine functions predicts a cool spell in the 2020s (Fig. 6b). The predicted final SAT anomaly for the next 2 decades is still rising (Fig. 6a) because of a warming secular non-linear trend (Fig. 6f). For the group of stations in central China,

Table 1. Coefficients (A, B, T) in a sine function (Eq. 1) for simulating 2 or 3 components of the SAT anomaly in 4 groups of Northeast China, North China, central China, and South China. IMF_3, IMF_4, IMF_5, and IMF_6 are 4 components of EEMD with timescales > 10 yr for the period 1924 to 2008. Coefficients of C_1, C_2, and C_3 in a 2nd-order polynomial function (Eq. 2) are used for simulating the components of secular non-linear trend. The correlations between each component of the SAT anomaly and its fitting curve are given in the fifth column. The total correlations between combination of 4 IMF components of the SAT anomaly and sum of all fitting curves are given in the sixth column in **bold**

Component(s)	A	B	T	Correlation	Total correlation
Northeast China					
IMF_3	0.0052	0.2354	16.02	0.73	**0.99**
IMF_4	0.0214	0.2096	32.04	0.85	
IMF_6 + IMF_5 (Trend)	C_1 = 421.2565	C_2 = −0.4643	C_3 = 0.00012713	0.9989	
North China					
IMF_3	0.0193	−0.1936	18.37	0.75	**0.97**
IMF_4	0.0124	−0.1376	29.96	0.81	
IMF_5	−0.061	−0.1474	67.31	0.97	
IMF_6 (Trend)	C_1 = 1034.3	C_2 = −1.0644	C_3 = 0.000274	0.999991	
Central China					
IMF_3	0.0092	0.1315	19.00	0.69	**0.97**
IMF_4	−0.0138	0.1780	56.83	0.86	
IMF_5	−0.0891	0.2839	87.10	0.99	
IMF_6 (Trend)	C_1 = 884.2499	C_2 = −0.9071	C_3 = 0.0002326	0.99996	
South China					
IMF_3	−0.00019	0.1702	12.89	0.60	**0.96**
IMF_4	0.0226	-0.2410	35.87	0.94	
IMF_5	−0.0042	-0.0536	45.84	0.95	
IMF_6 (Trend)	C_1 = 350.2646	C_2 = −0.3711	C_3 = 0.000098	0.99997	

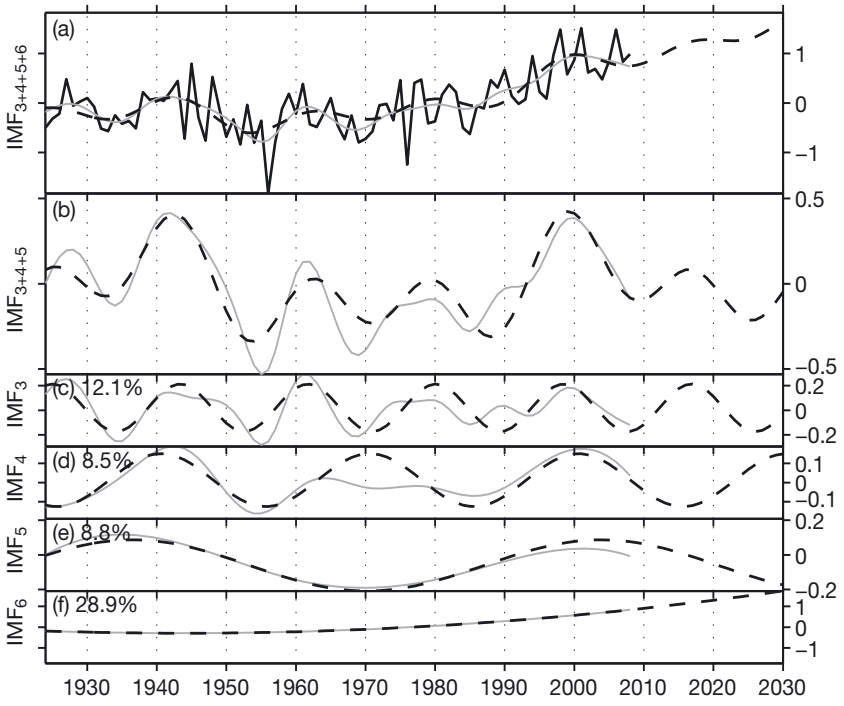

Fig. 6. Same as in Fig. 4 except of the original annual-mean SAT anomaly series averaged using 4 station series in North China from 1924 to 2008 and a prediction from 2009 to 2030 (dashed line). Three sine functions are used in (c) to (e), and a 2nd-order polynomial function is used in (f)

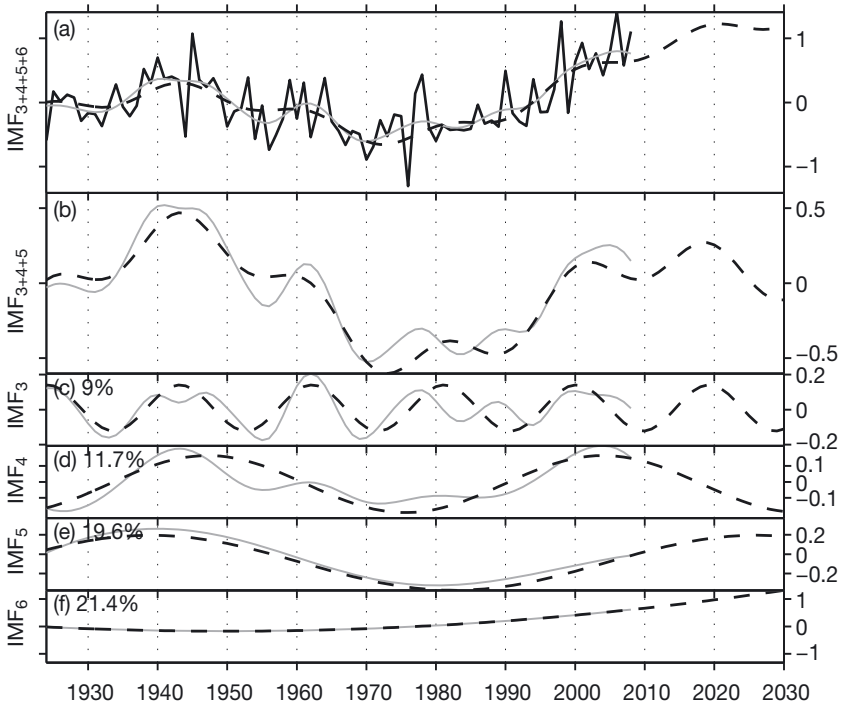

Fig. 7. Same as in Fig. 6 except of the original annual-mean SAT anomaly series averaged using 6 station series in central China (Yangtze River) from 1924 to 2008 and a prediction from 2009 to 2030 (dashed line)

the prediction produced by combining the 3 sine functions indicates a warm flat near the year 2018 (Fig. 7b). Thus, the predicted final SAT anomaly for the next 2 decades in the central China will have a high stage that exceeds any period in the last century (Fig. 7a). In the group of stations from South China, the prediction from combining 3 inter-decadal sine functions projects a cool spell during 2015 to 2025 (Fig. 8b). The predicted final SAT anomaly in South China for the next decade maintains the current level and then shows a quick warming process in 2020s (Fig. 8a).

5. DISCUSSION AND CONCLUSIONS

With the 18 station SAT anomaly data in eastern China from 1921 to 2011, 16 stations were used and categorized into 4 regional groups in Northeast China, North China, Central China, and South China. The method of EEMD was applied to examine internal multi-timescale variability and secular non-linear trends of each regional SAT anomaly series. Four regional differences in multi-timescale variability, secular non-linear trends, and their predictions of SAT anomaly are highlighted as follows.

A consistent secular warming trend with an average rate of 3.3°C per century was observed in Northeast China from the 3 stations of Hailar, Harbin, and Shenyang. These 3 stations were categorized as a group based on their similarities in geographical location and regional warming trend. Another group in North China consists of Qingdao, Taiyuan, Tianjin, and Beijing stations, experiencing a slight cooling trend before the 1950s and a warming trend since the 1960s. The station of Hohehot was excluded from any group because its secular trend of SAT anomaly is abnormal and different from that of the 2 groups in Northeast China and North China. In southern China including the Yangtze River basin and South China, secular non-linear trends of SAT anomaly at 9 stations showed a slight cooling

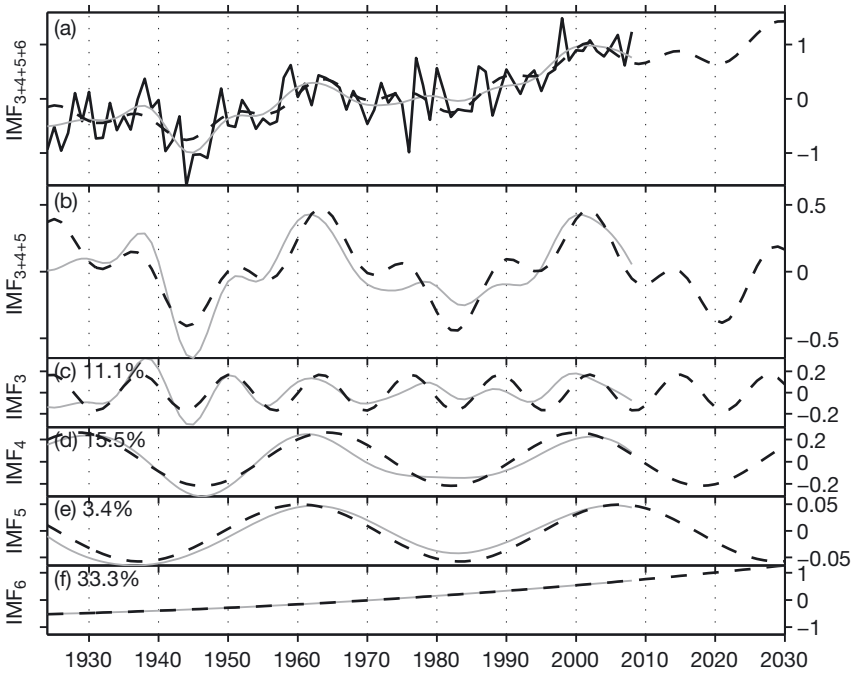

Fig. 8. Same as in Fig. 6 except of the original annual-mean SAT anomaly series averaged using 3 station series in South China from 1924 to 2008 and a prediction from 2009 to 2030 (dashed line)

trend or a weak warming trend before the 1950s and a continuous warming trend after the 1960s, except for the station of Kunming with a strong warming trend from 1924 to 2008. After removing the Kunming station located at the Yunnan-Guizhou Plateau, 2 groups of stations in central China (along the Yangtze River) and South China were defined according to their own evolution in multi-timescale variability.

Multi-timescale SAT anomaly variations for the 2 groups of central China and North China showed the warmest spell in the 1940s, while there was a cool spell in the 2 groups of South China and Northeast China. This means that the 2 river basins, the Yangtze and Yellow River, were warmer in the 1940s, while it was cooler in Northeast China and South China. The second warm spell existed in the 3 groups of North China, central China, and South China from the late 1990s to the early 2000s. A longer warm spell maintained in the recent 2 decades in Northeast China, particularly for the Hailar station. Multi-timescale variations of SAT-anomaly variability, including the quasi-22-yr and quasi-65-yr oscillations detected in previous studies (e.g. Wang et al. 1991, Schlesinger & Ramankutty 1994, Qian & Lu 2010), were also found in this study.

A secular warming trend commonly exists in eastern China particularly since the 1960s. In the 4 regions, the largest warming trends appeared in Northeast China and North China with rates of 3.3°C per century and 1.21°C per century, respectively. This secular warming trend is commonly attributed to anthropogenic activity. In China, the current secular warming trend is expected to continue due to rapid and persistent urbanization. As studied by Ren et al. (2008), urbanization effects on observed SAT-anomaly trends in North China are obvious, with a warming comparison between 0.16°C per decade in a large-city group and 0.07°C per decade in a small-city group. Therefore, our prediction for the secular trend in the coming decades might not have large bias error. However, this trend does not occur in the wide rural areas, as shown in the Beijing rural and mountain regions. For the decade of 1998 to 2008, 4 large site trends of –0.40, –0.32, –0.34, and –0.32°C belong to 10 cooling stations located in the Beijing rural and mountain stations, while another 10 warming stations with 4 large site trends of 0.24, 0.23, 0.12, and 0.11°C (Beijing station) are situated in the Beijing urban area (Qian & Li 2012). Therefore, we need to pay attention particularly to the future tendency of multi-timescale variation in all 4 regions because it may indicate a climate change in wide rural areas. In Northeast China, the natural SAT anomaly will have a cold peak in this decade and then a warm peak in the next decade. In North China, the natural SAT anomaly will have 2 cooling decadal steps after the warm decadal flat centered on 2000. In central China, the natural SAT anomaly will have a warm peak in this decade and then a cold peak late in the next decade. In South China, the natural SAT anomaly will have a cold peak from this decade to the next decade. Although there is a secular warming trend, the predicted SAT anomaly in Northeast China is expected to continue the recent warming slowdown in this decade and then show a new warm flat in the next decade. The predicted final SAT anomaly for the next decade in North China will have a slight warming trend. The predicted final SAT anomaly for the next 2 decades in central China will have a warm spell that exceeds any warm flat in the last century. A similar result of the annual-mean temperature increase in the Yangtze River Valley for the period 2001 to 2040 was

also documented by Orlowsky et al. (2010) using a statistical analog resampling scheme. The predicted final SAT anomaly for the next decade in South China will likely maintain the current level in this decade then have a quick warming process in the 2020s. The seasonal SAT variability particularly in winter and summer in China is also an interesting target for future research.

Acknowledgements. The authors thank the editor and 3 anonymous reviewers for their valuable comments and suggestions, which improved the paper. This work was supported by the Strategic Priority Research Program of the Chinese Academy of Sciences (XDA05090407) and the National Natural Science Foundation of China (41375073). Dr. J. Du of EMC/NCEP is appreciated for his help improving the readability of the manuscript.

LITERATURE CITED

Allan RJ, Lindesay JA, Reason C (1995) Multidecadal variability in the climate system over the Indian Ocean region during the austral summer. J Clim 8:1853–1873

Barlow M, Nigam S, Berbery EH (2001) ENSO, Pacific decadal variability, and US summertime precipitation, drought, and stream flow. J Clim 14:2105–2128

Bordi I, Fraedrich K, Jiang JM, Sutera A (2004) Spatio-temporal variability of dry and wet periods in eastern China. Theor Appl Climatol 79:81–91

Cao LJ, Zhao P, Yan ZW, Jones P, Zhu YN, Yu Y (2013) Instrumental temperature series in eastern and central China back to the nineteenth century. J Geophys Res 118:8197–8207

Delworth TL, Mann ME (2000) Observed and simulated multidecadal variability in the Northern Hemisphere. Clim Dyn 16:661–676

Enfield A, Trimble P (2001) The Atlantic multidecadal oscillation and its relation to rainfall and river flows in the continental US. Geophys Res Lett 28:2077–2080

Foster G, Rahmstorf S (2011) Global temperature evolution 1979–2010. Environ Res Lett 6:044022

Fu CB, Qian C, Wu ZH (2011) Projection of global mean surface air temperature changes in next 40 years: uncertainties of climate models and an alternative approach. Sci China Earth Sci 54:1400–1406

Gao XQ, Zhang X, Qian WH (2006) Climate change: long-term trends and short-term oscillations. J Trop Meteorol 12:139–149

Hoerling M, Hurrell J, Kumar A, Terray L and others (2011) On North American decadal climate for 2011–2020. J Clim 24:4519–4528

Huang NE, Shen Z, Long SR, Wu ML and others (1998) The empirical mode decomposition and the Hilbert spectrum for nonlinear and non-stationary time series analysis. Proc R Soc Lond A 454:903–995

Hurrell JW, Delworth T, Danabasoglu G, Drange H and others (2010) Decadal climate prediction: opportunities and challenges. In: Hall J, Harrison DE, Stammer D (eds) Proceedings of OceanObs'09: sustained ocean observations and information for society, Vol 2, Venice, 21–25 September 2009. ESA Publication WPP-306, doi:10.5270/OceanObs09.cwp.45

Keenlyside NS, Latif M, Jungclaus J, Kornblueh L, Roeckner E (2008) Advancing decadal-scale climate prediction in the North Atlantic sector. Nature 453:84–88

Kerr RA (2009) What happened to global warming? Scientists say just wait a bit. Science 326:28–29

Kosaka Y, Xie SP (2013) Recent global-warming hiatus tied to equatorial Pacific surface cooling. Nature 501:403–407

Li JP, Sun C, Jin FF (2013) NAO implicated as a predictor of Northern Hemisphere mean temperature multi-decadal variability. Geophys Res Lett 40:5497–5502

Li Q, Ren RC, Cai M, Wu GX (2012) Attribution of the summer warming since 1970s in Indian Ocean Basin to the inter-decadal change in the seasonal timing of El Niño decay phase. Geophys Res Lett 39:L12702, doi:10.1029/2012GL052150

Li SL, Bates G (2007) Influence of the Atlantic Multidecadal Oscillation (AMO) on the winter climate of East China. Adv Atmos Sci 24:126–135

Lin XC, Yu SQ, Tang GL (1995) Series of average air temperature over China for the last 100-year period. Sci Atmos Sin 19:525–534 (in Chinese)

Mantua NJ, Hare SR, Zhang Y, Wallace JM, Francis RC (1997) A Pacific interdecadal climate oscillation with impacts on salmon production. Bull Am Meteorol Soc 78: 1069–1079

Meehl GA, Goddard L, Murphy J, Stouffer RJ and others (2009) Decadal prediction: Can it be skillful? Bull Am Meteorol Soc 90:1467–1485

Mochizuki T, Ishii H, Kimoto M (2010) Pacific decadal oscillation hindcasts relevant to near-term climate prediction. Proc Natl Acad Sci USA 107:1833–1837

Murphy J, Kattsov V, Keenlyside N, Kimotod M and others (2010) Towards prediction of decadal climate variability and change. Procedia Environ Sci 1:287–304

Orlowsky B, Bothe O, Fraedrich K, Gerstengarbe FW, Zhu X (2010) Future climates from bias-bootstrapped weather analogues: an application to the Yangtze River basin. J Clim 23:3509–3524

Pohlmann H, Johann HJ, Köhl A, Stammer D, Marotzke J (2009) Initializing decadal climate predictions with the GECCO oceanic synthesis: effects on the North Atlantic. J Clim 22:3926–3938

Pu B, Wen XY, Wang SW, Zhu JH (2007) Diagnostic and modeling study of the two basic modes of surface air temperature and its variation in China. Adv Earth Sci 22:456–467 (in Chinese)

Qian C, Wu ZH, Fu CB, Zhou TJ (2010) On multi-timescale variability of temperature in China in modulated annual cycle reference frame. Adv Atmos Sci 27:1169–1182

Qian WH, Li J (2012) A slowing-down period during the long-term warming in the Beijing region. Adv Clim Chang Res 8:178–182 (in Chinese)

Qian WH, Lu B (2010) Periodic oscillations in millennial global-mean temperature and their causes. Chin Sci Bull 55:4052–4057

Qian WH, Lu B, Zhu CW (2010) How would global-mean temperature change in the 21st century? Chin Sci Bull 55:1963–1967

Rayner NA, Parker DE, Horton EB, Folland CK and others (2003) Global analyses of sea surface temperature, sea ice, and night marine air temperature since the late nineteenth century. J Geophys Res D 108:4407, doi:10.1029/2002JD002670

Ren G, Zhou Y, Chu Z, Zhou J, Zhang A, Guo J, Liu X (2008) Urbanization effects on observed surface air temperature

trends in North China. J Clim 21:1333–1348
Salinger MJ (2005) Climate variability and change: past, present and future–an overview. Clim Change 70:9–29
Scafetta N, West BJ (2008) Is climate sensitive to solar variability? Phys Today 61:50–51
Schlesinger ME, Ramankutty N (1994) An oscillation in the global climate system of period 65–70 years. Nature 367:723–726
Smith DM, Cusack S, Colman AW, Chris KF, Glen RH, Murphy JM (2007) Improved surface temperature prediction for the coming decadal from a global climate model. Science 317:796–799
Stainforth DA, Allen MR, Tredger ER, Smith LA (2007) Confidence, uncertainty and decision-support relevance in climate predictions. Philos Trans R Soc Lond A 365: 2145–2161
Stocker TF, Qin DH, Plattner GK, Tignor MMB and others (2013) Climate change 2013: the physical science basis. Intergovernmental Panel on Climate Change, Working Group I Contribution to the IPCC Fifth Assessment Report (AR5), Cambridge University Press, New York, NY
Sutton RT, Hodson D (2007) Climate response to basin-scale warming and cooling of the North Atlantic Ocean. J Clim 20:891–907
Tang GL, Lin XC (1992) Average air temperature series and its variations in China. Meteorol Mon 18:3–6 (in Chinese)
Tao S, Fu C, Zeng Z, Zhang Q, Kaiser D (1991) Two long-term instrumental climatic data bases of the People's Republic of China. ORNL/CDIAC-102, NDP-039/R1, Oak Ridge National Laboratory, Oak Ridge, TN, ftp://cdiac.esd.ornl.gov/pub/ndp039/ndp039.txt
Taylor KE, Stouffer RJ, Meehl GA (2012) An overview of CMIP5 and the experiment design. Bull Am Meteorol Soc 93:485–498
Tung KK, Zhou J (2013) Using data to attribute episodes of warming and cooling in instrumental records. Proc Natl Acad Sci USA 110:2058–2063
Wang B, Liu M, Yu Y, Li LJ and others (2013) Preliminary evaluations of FGOALS_g2 for decadal predictions. Adv Atmos Sci 30:674–683
Wang RS, Wang SW, Fraedrich K (1991) An approach to reconstruction of temperature on a seasonal basis using historical documents from China. Int J Climatol 11: 381–392
Wang SW (1990) Variations of temperature in China for the 100 year period in comparison with global temperatures. Meteorol Mon 16:11–15 (in Chinese)
Wang SW, Ye JL, Gong DY, Zhu JH (1998) Construction of mean annual temperature series for the last one hundred years in China. J Appl Meteorol Sci 9:392–401 (in Chinese)
Wang SW, Zhu JH, Cai JN (2004) Interdecadal variability of temperature and precipitation in China since 1880. Adv Atmos Sci 21:307–313
Wang YG, Gong ZS, Xu L, Ai WX (2005) Analysis of long trend of temperature and prediction in China and its influencing factors. J Applied Meteorol Sci 16:85–91 (in Chinese)
Wang YM, Li SL, Luo DH (2009) Seasonal response of Asian monsoonal climate to the Atlantic Multidecadal Oscillation. J Geophys Res 114:D02112, doi:10.1029/2008JD010929
Wu Z, Huang NE (2009) Ensemble empirical mode decomposition: a noise-assisted data analysis method. Adv Adapt Data Anal 1:1–41
Wu Z, Huang NE, Wallace JM, Smoliak B, Chen X (2011) On the time-varying trend in global-mean surface temperature. Clim Dyn 37:759–773
Yan Z, Yang C, Jones PD (2001) Influence of inhomogeneity on the estimation of mean and extreme temperature trends in Beijing and Shanghai. Adv Atmos Sci 18: 309–322
Zhao P, Jones P, Cao LJ, Yan ZW and others (2014) Trend of surface air temperature in eastern China and associated large-scale climate variability over the last 100 years. J Clim 27:4693–4703
Zhou JS, Tung KK (2013) Deducing multidecadal anthropogenic global warming trends using multiple regression analysis. J Atmos Sci 70:3–8
Zhu X, Fraedrich K, Wang W (2013) Future climate in the Tibetan Plateau from a statistical regional climate model. J Clim 26:10125–10138

Editorial responsibility: Gouyu Ren, Beijing, China

Submitted: March 18, 2014; Accepted: December 29, 2014
Proofs received from author(s): March 4, 2015